land

MDPI

Article

Effects of Climate Change and Human Activities on Streamflow in Arid Alpine Water Source Regions: A Case Study of the Shiyang River, China

Honghua Xia [1,2], Yingqing Su [1], Linshan Yang [1,*], Qi Feng [1], Wei Liu [1] and Jian Ma [3]

[1] Key Laboratory of Ecological Safety and Sustainable Development in Arid Lands, Northwest Institute of Eco-Environment and Resources, Chinese Academy of Sciences, Lanzhou 730000, China; xiahonghua@nieer.ac.cn (H.X.); yingqingsu@nieer.ac.cn (Y.S.); qifeng@lzb.ac.cn (Q.F.); weiliu@lzb.ac.cn (W.L.)
[2] University of Chinese Academy of Sciences, Beijing 100049, China
[3] Zhangye Forestry Research Institute, Zhangye 734000, China; majian0211@nieer.ac.cn
* Correspondence: yanglsh08@lzb.ac.cn

Abstract: Climate change and human activities were identified as the primary drivers of streamflow in arid alpine regions. However, limitations in observational data have resulted in a limited understanding of streamflow changes in these water sources, which hinders efforts to adapt to ongoing climate change and to formulate effective streamflow management policies. Here, we use the four main tributaries in the upper reach of the Shiyang River in China as a case study to investigate the long-term trends in streamflow within arid alpine water sources, quantifying the individual contributions of climate change and human activities to these changes. The findings revealed that temperatures and precipitation in arid alpine regions have risen over the past 40 years. Although the warming trend has been significant, it has slowed in recent years. Nevertheless, three-quarters of the rivers are experiencing a decline in streamflow. The land types within the watershed remain relatively stable, with land use and cover change (LUCC) primarily occurring in the Gulang River watershed. Climate change has significantly affected streamflow change in high and rugged terrains, with an influence exceeding 70%. For example, Jingta River showed an impact of 118.79%, Zamu River 84.00%, and Huangyang River 71.43%. Human-driven LUCC, such as the expansion of cultivated and urban land, have led to increased water consumption, resulting in reduced streamflow. This effect is particularly pronounced in the low-lying and gently undulating areas of the Gulang River, where LUCC account for 78.68% of the change in streamflow. As human activities intensify and temperatures continue to rise, further declines in streamflow are projected, highlighting the urgent need for effective water resource management. These insights highlight the urgent need for targeted mitigation and adaptation strategies to confront the water scarcity challenges faced by these vulnerable regions.

Keywords: streamflow; climate change; land use and cover change; SWAT model; arid alpine water source regions

Citation: Xia, H.; Su, Y.; Yang, L.; Feng, Q.; Liu, W.; Ma, J. Effects of Climate Change and Human Activities on Streamflow in Arid Alpine Water Source Regions: A Case Study of the Shiyang River, China. *Land* **2024**, *13*, 1961. https://doi.org/10.3390/land13111961

Academic Editors: Xiaowei Guo, Charles Bourque and Licong Dai

Received: 2 November 2024
Revised: 14 November 2024
Accepted: 17 November 2024
Published: 20 November 2024

1. Introduction

Climate change and human activities have significantly impacted terrestrial streamflow [1–3]. Climate change brought about changes in key meteorological factors such as temperature, precipitation, and evapotranspiration, which inevitably affected streamflow patterns [4–6]. Additionally, human activities—including land use and land cover change (LUCC), dam management, and groundwater extraction—also played a crucial role in reshaping these dynamics [7–9]. Over the past five years, global streamflow generally remained below normal levels, with 2023 recognized as the driest year for rivers worldwide in over thirty years [10]. The rising frequency of extreme weather events (e.g., droughts and heavy precipitation) has worsened hydrological extremes globally, leading to increased

water scarcity and tension [10]. This situation underscores the urgent need for adaptive management strategies for streamflow to tackle ongoing challenges stemming from climate change and human activities.

Understanding how climate change and human activities contribute to streamflow is essential for effective management [11]. Recently, there has been considerable interest and funding in the management of streamflow. However, debates persist regarding trends and the driving factors behind changes in streamflow. For instance, Zhang et al. found that changes in vegetation cover due to climate change would further amplify the effects of climate change on streamflow, and the cumulative effects of climate change should be emphasized in studies [4]. Tan et al., using the Budyko framework to analyze 96 watersheds in Canada, concluded that human activities have a more significant impact on streamflow than climate change [5]. Sadra et al., in their study of the Ferson Creek watershed in the United States, found that the streamflow in this watershed is particularly sensitive to land use changes, especially forest cover changes [7]. Furthermore, some studies suggest that the negative effects of climate change—especially from potential evapotranspiration—have led to a more severe decline in streamflow than previously thought [11–13], while others argue that human land use changes might increase streamflow [6,14,15]. A review of the existing research reveals considerable divergence in discussions about the driving factors of streamflow change. These disagreements often arise from differences in data resolution [12], inadequate measurement tools, short or inconsistent flow records [13], and restrictive data-sharing policies [16], which hinder a complete understanding of streamflow change.

Clarifying historical changes in streamflow is vital for grasping its dynamics and improving the accuracy of future predictions [17]. The formation of streamflow involves complex processes, such as precipitation infiltration, water movement in the unsaturated zone, and groundwater contributions. Mathematical statistics, chemical tracing, and hydrological models are commonly used methods to study the impact of climate change and human activities on streamflow in arid and alpine regions [18]. However, the formation process of streamflow is inherently complex and nonlinear, and a single mathematical statistical method is insufficient to reveal the complex relationship between streamflow and multiple driving factors [6]. Chemical tracing methods to observe base flow can be time-consuming and labor-intensive, making large-scale studies in extreme environments (e.g., cold and arid regions) particularly challenging [17]. Hydrological models typically simplify streamflow processes [18–20]. The Soil and Water Assessment Tool (SWAT) model is capable of handling different climate and LUCC scenarios and has gained popularity for its accuracy in simulating regional precipitation/streamflow processes [21–26].

Arid alpine regions are crucial water sources in global drylands, playing a crucial role in regulating the hydrological cycle and sustaining ecological balance [1–3]. These water sources are sensitive to both climate change and human activities, yet our understanding of how factors like precipitation and evapotranspiration affect streamflow is still limited [2,27]. This gap in knowledge hinders effective streamflow management and socio-economic development in these areas [28,29]. Currently, there is an urgent need to study the hydrological processes in arid alpine regions. Therefore, we have chosen the four main tributaries in the upper reach of the Shiyang River as a case study to develop targeted strategies that address water shortages.

The specific objectives of this study were to (1) analyze long-term changes in streamflow from water sources in arid alpine regions; (2) determine the contributions of climate change and human activities to streamflow in these areas; and (3) develop adaptive streamflow management policies for arid alpine water sources. The findings are expected to provide valuable insights for managing streamflow in these critical regions.

2. Methods and Materials

2.1. Study Area

To investigate changes in streamflow in arid alpine water sources, we selected four major tributaries of the Shiyang River in northwestern China as case studies: the Jinta

(JT) River, the Zamu (ZM) River, the Huangyang (HY) River, and the Gulang (GL) River (Figure 1). This region lies at the edge of the Tibetan Plateau, with elevations ranging from 1870 m to 4859 m. The average annual temperature varied between 2 °C and 8 °C, while annual evaporation levels ranged from 2000 mm to 3000 mm, and the long-term average precipitation fluctuated between 237 mm and 628 mm. The study area encompasses four hydrological stations: Nanyingshuiku (NYSK), Zamusi (ZMS), Jinshatai (JST), and Gulang (GL). Precipitation data are collected at Nanyingshuiku (NYSK), Maozangsi (MZS), Haxi (HX), and Longgou (LG), which correspond to the streamflow and precipitation measurements for the JT River, ZM River, HY River, and GL River, respectively. Additionally, the meteorological stations include Nanyingshuiku (NYSK), Menyuan (MY), Wuwei (WW), and Wushaoling (WSL).

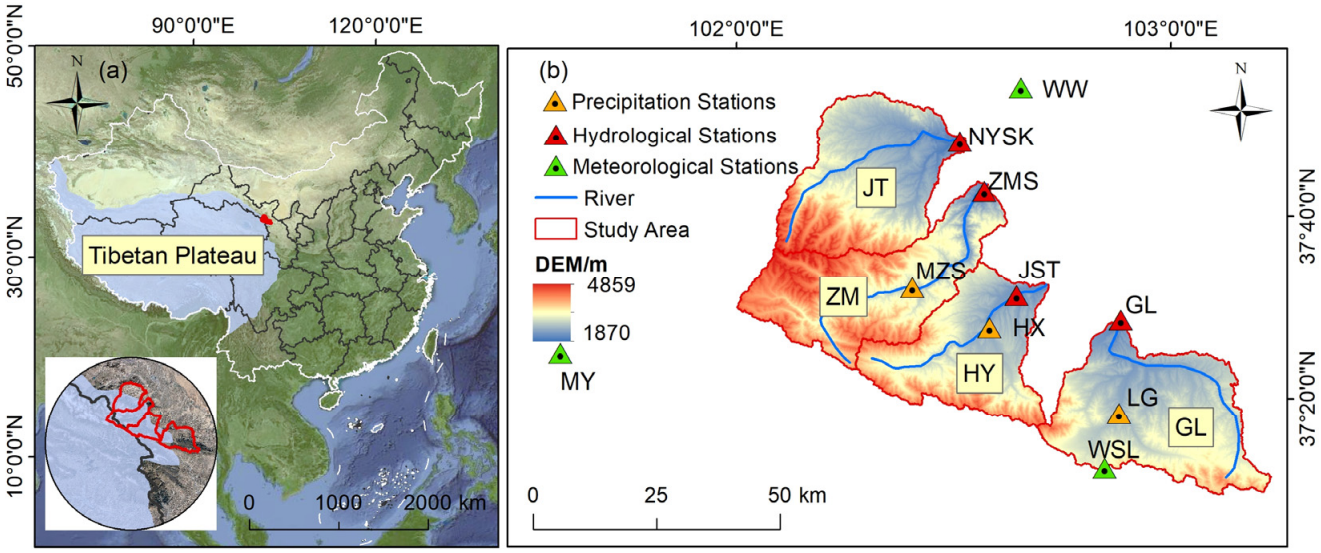

Figure 1. Location of the study area. (**a**) The geographical position of the watershed in China. (**b**) The environmental background. The abbreviations featured in the figure are listed in Supplementary Material Table S1.

The watershed experienced escalating conflicts over water resources due to climate change and human activities, resulting in heightened water scarcity and uneven temporal and spatial distribution, which worsened ecological issues in the area [30]. Consequently, we chose this region to explore streamflow change in similar environments, aiming to identify the impacts of climate change and human activities on watershed water resources. This research ultimately provides critical insights for the scientific management of water resources in arid alpine regions.

2.2. Methods

2.2.1. Research Framework

This study developed a quantitative analysis framework to assess the changes in streamflow in arid alpine regions under various climate change scenarios and human activities. By inputting different climate and LUCC combination scenarios into the SWAT model to simulate runoff, and using the formula proposed by Yang et al. [31], we quantified the differences in the impacts of climate change and human disturbances on streamflow, identified the key influencing factors, and proposed corresponding adaptive management strategies (Figure 2).

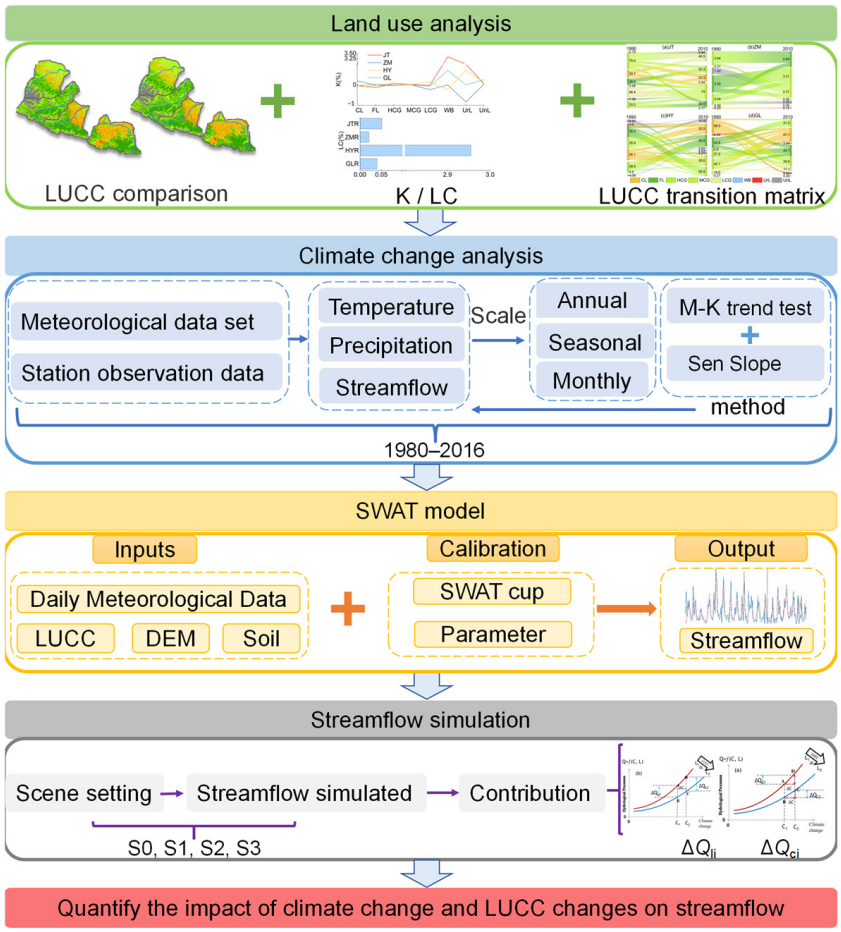

Figure 2. Research framework on the effects of climate change and human activities on streamflow.

2.2.2. Trend Analysis Method

Sen's slope method is used to quantify the magnitude of hydrometeorological change trends. It is less affected by missing data or outliers and is not influenced by the evenness or oddness of the data. This makes it highly adaptable for reflecting trends in data changes. As a result, Sen's slope is commonly used to study hydrological change.

The Mann–Kendall (M-K) trend test is used to analyze the characteristics and significance of hydrometeorological changes within the watershed. This method determines the significance of climate change trends by calculating the z-value. When $|z| \geq 1.96$, the trend is considered significant at the 95% confidence level, and when $|z| \geq 2.58$, the trend is considered significant at the 99% confidence level.

The detailed calculation process for Sen's slope method and the M-K test is provided in the literature [32,33].

2.2.3. Pearson Correlation Coefficient

The linear relationship between two variables, x and y, can be expressed as the ratio of the covariance between the two variables to the product of their standard deviations, which is known as the Pearson correlation coefficient [34]. The formulation is as follows:

$$r = \frac{\sum_{i=1}^{n}(x_1 - \overline{x})(y_1 - \overline{y})}{\sqrt{(x_1 - \overline{x})^2}\sqrt{(y_1 - \overline{y})^2}} \quad (1)$$

The Pearson correlation coefficient ranges from -1 to 1, with larger absolute values indicating a stronger correlation.

2.2.4. Analysis of LUCC

The LUCC dataset we used consists of 30 m resolution remote sensing imagery provided by the Data Center for Resources and Environmental Sciences of the Chinese Academy of Sciences, visit the website http://www.resdc.cn, accessed on 20 June 2022. This dataset includes land use monitoring data from 1990 and 2010, based on Landsat remote sensing image interpretation. We categorize LUCC types into eight main categories, which include cultivated land (CL), forest land (FL), water body (WB), urban land (UrL), unutilized land (UnL), high-coverage grassland (HCG), medium-coverage grassland (MCG), and low-coverage grassland (LCG). We applied the land use dynamic degree and the land use transition matrix to reveal the LUCC dynamics within the watershed [35,36]. The land use dynamic degree includes the single land use dynamic degree (K) and the comprehensive land use dynamic degree (LC), which indicate the extent of change in land use types over a specific period. A higher value reflects a more significant LUCC. The formulation is as follows:

$$K = \frac{U_b - U_a}{U_a} \times \frac{1}{T} \times 100\% \quad (2)$$

$$LC = \left(\frac{\sum_{i=1}^{n} \Delta LU_{i-j}}{2\sum_{i=1}^{n} \Delta LU_i} \right) \times \frac{1}{T} \times 100\% \quad (3)$$

$$S_{ij} = \begin{bmatrix} S_{11} & S_{12} & \cdots & S_{1n} \\ S_{21} & S_{22} & \cdots & S_{2n} \\ \vdots & \vdots & \vdots & \vdots \\ S_{n1} & S_{n2} & \cdots & S_{nn} \end{bmatrix} \quad (4)$$

where U_a and U_b represent the area of land use type U at the beginning (a) and the end (b) of the study period, respectively; T represents the study period (years); LU_i represents the area of land use type i at the beginning of the study; $\Delta LU_{i\text{-}j}$ represents the absolute value of the area converted from land use type i to type j; S represents the area (km^2); n represents the total number of LUCC types; and i and j correspond to the LUCC types at the start and conclusion of the study period, respectively.

2.2.5. SWAT Model Construction and Calibration

The SWAT (Version 10.2) model was used to simulate streamflow in watersheds [24]. This model is built on the water balance equation and is known for requiring fewer input parameters, providing superior spatial visualization, and yielding more reliable simulation results compared to other hydrological models [24,37]. The water balance equation used in the SWAT model is as follows:

$$SW_t = SW_0 - SW_s \quad (5)$$

$$SW_s = \sum_{i=1}^{t} \left(R_{day} - Q_{surf} - E_a - W_{seep} - Q_{gw} \right) \quad (6)$$

where SW_t represents the soil's water content at the end of the period, while SW_0 denotes the soil's water content at the start of the period. SW_s signifies the cumulative value of the differences among precipitation (R_{day}), surface streamflow (Q_{surf}), evapotranspiration (E_a), soil profile infiltration into the vadose zone (W_{seep}), and groundwater regression flow (Q_{gw}) over the time period t. All these physical quantities are measured in millimeters (mm).

During the calibration of the model, we employed the SUFI-2 within the SWAT Cup. For the JT River, ZM River, and HY River, we defined the calibration period as 1985 to 2000 and the validation period as 2001 to 2016. As for the GL River, the calibration period was set from 1989 to 2000, with the validation period extending from 2001 to 2006.

Through sensitivity analysis, the parameters significantly affecting streamflow for the four rivers were identified for calibration (Table S2). To comprehensively assess the

simulation performance of the model, we employed a suite of metrics to evaluate the accuracy of the simulation, including: the Nash–Sutcliffe Efficiency (*NSE*) to assess the model's goodness of fit, the Coefficient of Determination (R^2) to measure the model's ability to explain the variability in the data, the Kling–Gupta Efficiency (*KGE*), which takes into account bias, variance, and correlation, and the Percentage Bias (*PBIAS*) to gauge the degree of deviation between the model's predictions and observed values. Further details regarding the parameter settings and verification processes can be found in the Supplementary Materials (Test S1 and Table S2).

2.2.6. Setting of Simulation Scenarios

To effectively isolate the impacts of climate change and LUCC on streamflow in the study area, we considered the hydrological variations within the watershed. Based on two historical periods, 1985–2000 and 2001–2016, and corresponding LUCC data from 1990 and 2010, four scenarios were established for simulating streamflow using the SWAT model, as outlined in Table 1.

Table 1. Scenario setting and basis.

Scenario	Description	Climate	LUCC	Symbol
S0	Basic scenario	1985–2000	1990	$Q_{l_1}^{c_1}$
S1	Climate scenario	2001–2016	1990	$Q_{l_1}^{c_2}$
S2	LUCC scenario	1985–2000	2010	$Q_{l_2}^{c_1}$
S3	Comprehensive scenario	2001–2016	2010	$Q_{l_2}^{c_2}$

Note: Due to the lack of long-term streamflow measurement data for GLR, climate change is divided into two periods: 1989–2000 and 2001–2006.

S0: Utilizes meteorological data from 1985 to 2000 and LUCC data from 1990, serving as the baseline period for the study.
S1: Only the meteorological data are changed by using data from 2001 to 2016. This scenario isolates the effect of climate change on streamflow.
S2: Only the LUCC data are modified by using the 2010 LUCC data to assess the impact of LUCC on streamflow.
S3: Simultaneously alters both climate and LUCC data by using 2001–2016 meteorological data and 2010 LUCC data, aiming to study the combined effects of LUCC and climate change on streamflow.

2.2.7. Analytical Approaches for Attributing Streamflow Change

To elucidate the intricate nonlinear relationship arising from the interaction between LUCC and climate change, we adopted the method proposed by Yang et al. (2017) [31] to estimate the contribution of each factor to change in streamflow, distinguishing the individual contributions of LUCC and climate change, followed by attribution analysis. The method utilized the following formulas:

$$\Delta Q_{ci} = \frac{1}{2}\left[\left(Q_{li}^{i+1} - Q_{li}^{ci}\right) + \left(Q_{li+1}^{ci+1} - Q_{li+1}^{ci}\right)\right] \tag{7}$$

$$\Delta Q_{li} = \frac{1}{2}\left[\left(Q_{li+1}^{ci+1} - Q_{li}^{ci+1}\right) + \left(Q_{li+1}^{ci} - Q_{ci}^{ci}\right)\right] \tag{8}$$

$$\Delta Q_i = \Delta Q_{ci} + \Delta Q_{li} = Q_{li+1}^{ci+1} - Q_{li}^{ci} \tag{9}$$

$$\Delta Q_{ci} = \frac{1}{2}\left[\left(Q_{li}^{i+1} - Q_{li}^{ci}\right) + \left(Q_{li+1}^{ci+1} - Q_{li+1}^{ci}\right)\right] \tag{10}$$

$$Q_{ci} = \frac{\Delta Q_{ci}}{\Delta Q_i} \tag{11}$$

$$Q_{li} = \frac{\Delta Q_{li}}{\Delta Q_i} \quad (12)$$

where ΔQ_{li} represents the contribution of LUCC to streamflow, ΔQ_{ci} denotes the contribution of climate change to streamflow, and ΔQ_i indicates the combined contribution of LUCC and climate change to streamflow. Here, ΔQ_i reflects the specific contribution of both LUCC and climate change to streamflow. The indices i and $i + 1$ correspond to the data for the current and previous periods, respectively.

2.3. Data Sources

The data for this study primarily comprised remote sensing imagery, reanalysis products, and hydrological station observations and were used for LUCC and streamflow simulations. The measured precipitation and streamflow data are sourced from the aforementioned hydrological and precipitation stations. Daily temperature data were obtained from the Daily Values of the China Surface Climatological Data Dataset V3.0, and the dataset is publicly accessible at https://data.cma.cn/, accessed on 10 June 2022. Comprehensive information regarding data sources and preprocessing methodologies is available in the Supplementary Materials (Table S3).

3. Results

3.1. Streamflow Simulation Verification

In the SWAT model, we input hydrometeorological and LUCC data to calibrate parameters. Specifically, we collected daily T_{max} and T_{min} data from meteorological stations (NYSK, MY, WW, and WSL) and daily precipitation data from precipitation stations (NYSK, MZS, HX, and LG). Monthly data from four hydrological stations (NYSK, ZMS, JST, and GL) were used to simulate streamflow, representing the flow of the JT, ZM, HY, and GL Rivers, respectively. For meteorological parameters such as relative humidity, solar radiation, and wind speed, we relied on the built-in meteorological database (CFSR Global Weather Data) in the SWAT model for simulation. The calibration period for the JT, ZM, and HY Rivers was 1985–2000, with validation from 2001 to 2015. For the GL River, data were available only from 1989 to 2006, leading to a calibration from 1989 to 2000 and validation from 2001 to 2006.

The simulation results showed that modeled streamflow closely matched observed values, particularly for baseflow (Figure 3). The JT and ZM Rivers showed a good agreement between simulated and observed data in both periods, confirming reliability. The HY River had satisfactory calibration results, but validation was less favorable. Conversely, the GL River performed slightly worse due to its shorter simulation period. The performance assessment for both the simulation and calibration periods is shown in Table 2. Overall, it can be concluded that the model demonstrates satisfactory performance in simulating streamflow, indicating that the SWAT model is applicable in arid alpine water source regions.

Table 2. Performance evaluation for simulation and calibration periods.

Name	Calibration				Validation			
	R^2	NSE	PBIAS (%)	KGE	R^2	NSE	PBIAS (%)	KGE
JT River	0.81	0.81	6.4	0.84	0.73	0.72	−3.4	0.84
ZM River	0.82	0.80	5.0	0.89	0.74	0.70	10.3	0.81
HY River	0.79	0.78	−6.9	0.84	0.67	0.65	9.0	0.78
GL River	0.68	0.66	9.7	0.76	0.66	0.65	0.9	0.79

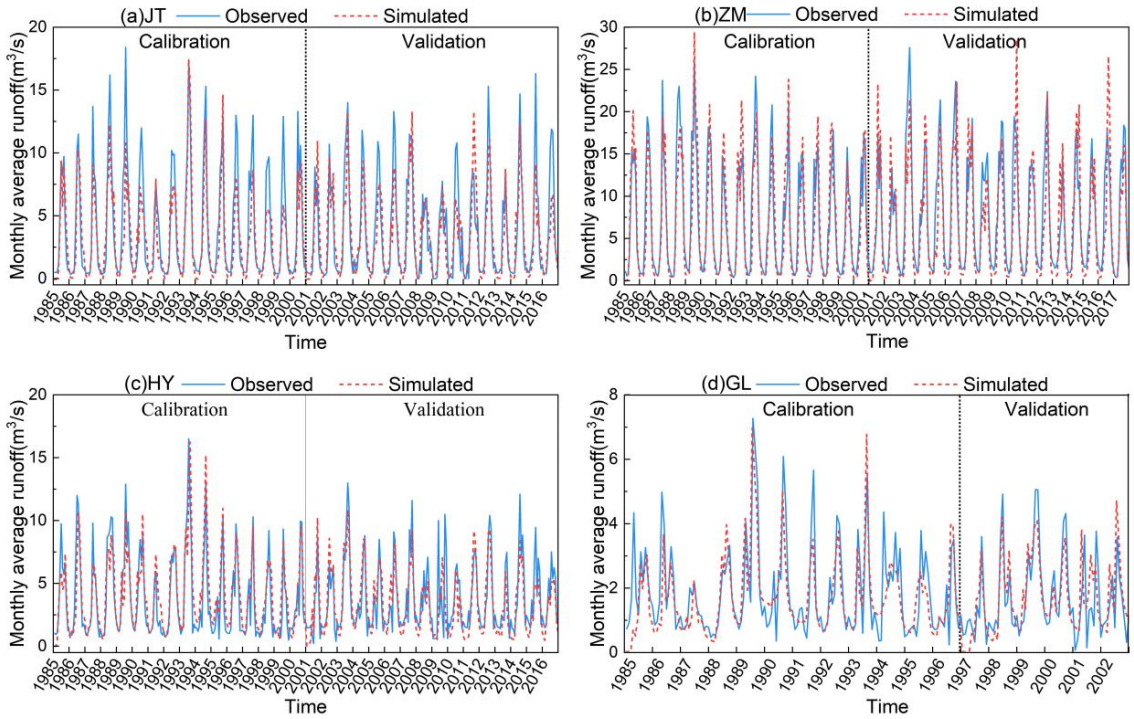

Figure 3. Comparison of streamflow simulated by SWAT model with monthly observation data of hydrologic stations during 1980–2016 in the JTR (**a**), ZMR (**b**), HYR (**c**), and GLR (**d**).

3.2. Analysis of LUCC Dynamics

Forest land and grassland dominated the study area, making up 28.8% and 40.6% of the land cover, respectively. Among the grasslands, high-coverage grassland accounted for 16.1%, medium-coverage grassland for 20.0%, and low-coverage grassland for 4.7%. Unused land represented 10.3%, while water body and urban land comprised 2.7% and 5.1%. Sub-basin analysis (Figure 4a,b) indicated that forest land was primarily located in the high-altitude areas of the ZM, HY, and GL Basin. In contrast, grassland was mainly found in the JT and ZM Basins. Cultivated land and urban land were concentrated at lower elevations near water bodies in the HY and GL Basins, while cultivated land was largely found in the upstream junctions of the JT and ZM Basins.

From 1990 to 2010, there was little change in LUCC and the single land use dynamic degree (Figure 4c) remained below 3.5%. Significant changes occurred in the water body and urban land categories, with the GL River Basin showing the highest dynamics, followed by the JT Basin. Overall, the comprehensive land use dynamic degree is generally lower than 0.05%, and the highest is not more than 3%, indicating stability in the watersheds (Figure 4d). According to the land use transfer matrix (Figure 5), changes included a loss of 75.6 km^2 of medium-coverage grassland in the JT Basin, with 39.6% transitioning to low-coverage grassland. The ZM Basin experienced a reduction of 50.7 km^2 of medium-coverage grassland, primarily converting to forest land. The HY Basin saw a decline of 36.9 km^2 of medium-coverage grassland, with 22.6% shifting to unutilized land. In the GL Basin, the most substantial change involved cultivated land, with 58.9 km^2 converted, 41.1% of which became medium-covered grassland.

Compared to 1990, the land types experiencing significant LUCC in the JT Basin in 2010 were unutilized land and medium-coverage grassland, with area changes of 2.35 km^2 and -2.21 km^2, respectively. In the ZM Basin, the changes in unutilized land and cultivated land were 2.35 km^2 and -1.61 km^2, respectively. The changes in other LUCC types, such as forest land, water body, urban land, and high-coverage grassland, were less than 1 km^2. In the HY Basin, the total LUCC area change was under 11 km^2, with the highest increase in high-coverage grassland at 0.67 km^2. In comparison to the other three sub-basins, the

GL Basin showed substantial changes in LUCC area, with grassland, cultivated, forest, and unutilized land changing by −2.49 km^2, 1.78 km^2, 1.93 km^2, and 1.08 km^2, respectively.

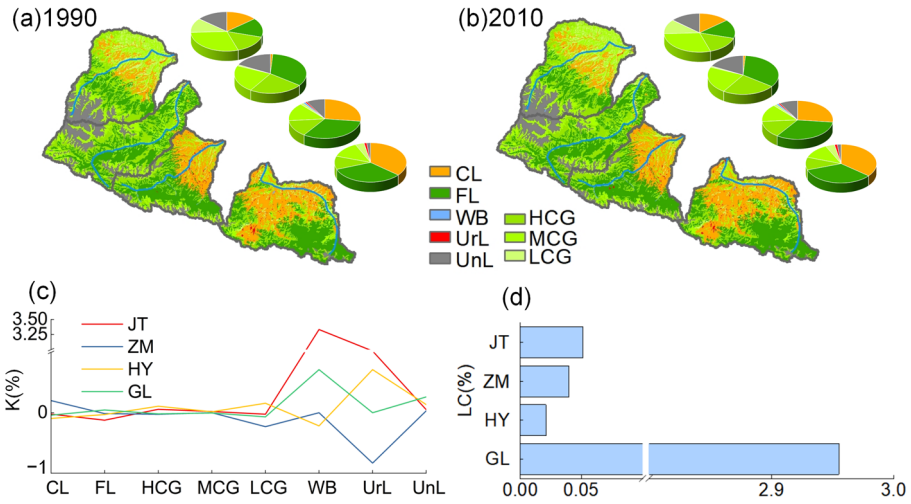

Figure 4. LUCC from 1990 to 2010. (**a**) and (**b**) represent the LUCC of the four basins for 1990 and 2010, respectively. (**c**) indicates the land use dynamic degree of the four basins. (**d**) refers to the comprehensive land use dynamic degree of the four basins. Note: The abbreviations CL, FL, WB, UrL, UnL, HCG, MCG, and LCG represent cultivated land, forest land, water body, urban land, unutilized land, high-coverage grassland, medium-coverage grassland, and low-coverage grassland, respectively.

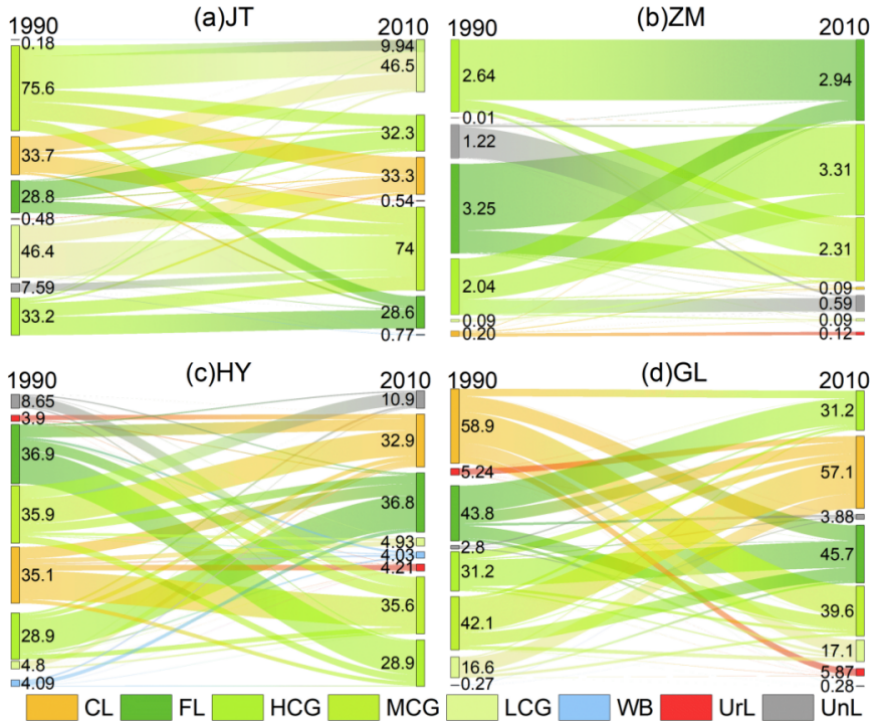

Figure 5. The 1990–2010 land use transition matrix in the JTR (**a**), ZMR (**b**), HYR (**c**), and GLR (**d**). The unit of LUCC transfer area is km^2.

3.3. Characteristics of Climate and Hydrological Factors

The study period was divided into two phases, T1 (1985–2000) and T2 (2001–2016), using 2000 as the dividing point to analyze meteorological and hydrological changes. During this time, annual average temperature and precipitation in the watershed exhibited different upward trends (Figure 6). Sen's slope for annual temperatures was positive,

with T1 slopes equal to or greater than those in T2; the warming trend in T1 was statistically significant and more pronounced. While the warming trend in T2 slowed, it persisted throughout the period. Temperatures at NYSK, MY, WW, and WSL increased at rates of 0.04 °C·a^{-1}, 0.05 °C·a^{-1}, 0.08 °C·a^{-1}, and 0.04 °C·a^{-1}, respectively. Except for JT River, Sen's slopes for precipitation were positive in both phases, with T2 showing a more pronounced trend. Despite JT River's negative slope in T2, the overall precipitation trend remained upward, with increases of 0.07 mm·a^{-1}, 0.80 mm·a^{-1}, 0.49 mm·a^{-1}, and 1.27 mm·a^{-1} for JT, ZM, HY, and GL Rivers, respectively. During T1, annual streamflow exhibited a decreasing trend, with ZM River declining while other stations showed increases. Across the entire period, only ZM River had an increasing streamflow trend, with changes of −0.01 m^3·s^{-1}a^{-1}, 0.01 m^3·s^{-1}a^{-1}, −0.01 m^3·s^{-1}a^{-1}, and −0.02 m^3·s^{-1}a^{-1} for JT, ZM, HY, and GL Rivers, respectively.

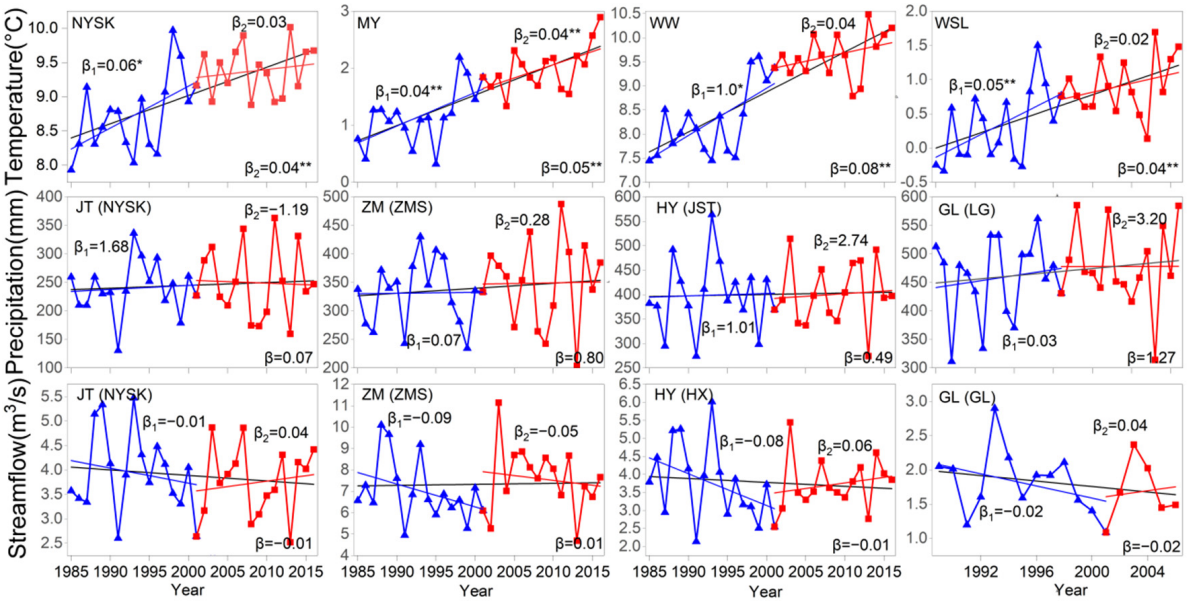

Figure 6. Changing trends in temperature, precipitation, and streamflow. Note: β1 and β2 represent Sen's slope during 1985–2000 and 2001–2016, respectively. "β" in bold denotes the trends for the entire period 1980–2009 (per decade). The single asterisk ("*") and two asterisks ("**"), represent statistical significance levels of $p < 0.1$and $p < 0.05$, respectively.

Seasonal trends (Figure 7) show that monthly precipitation typically declines in spring but increases in autumn and winter, while streamflow decreases in summer and rises in autumn. Temperature data indicate consistent monthly increases for MY and WW, with significant rises in MY from June to August and in WW during March, May to August, and November. NYSK experiences slight declines in January and December but significant increases from March to April and June to November, while WSL declines in December but rises significantly in June. JT River shows increased precipitation in January–February, July–October, and December, with ZM River increasing in January, April, and July–December. HY River has declines in March, May, July, and December. ZM River's streamflow decreases from February to September, with ZM and HY Rivers showing reductions from May to August but increases in other months. Overall, temperature trends are rising, and while precipitation shows slight declines in spring and summer, the overall trend is upward, aligning with annual averages. In contrast, JT and GL Rivers have more months of decreasing streamflow, while ZM River shows more months of significant increases, resulting in an upward trend in annual streamflow.

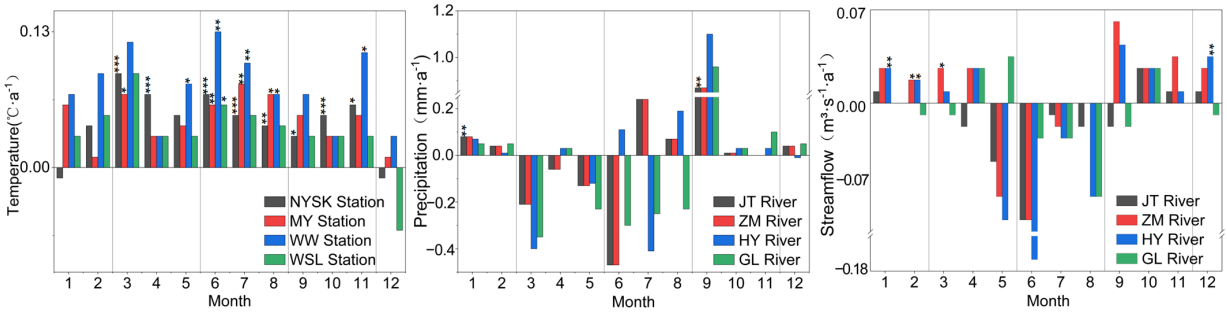

Figure 7. Sen's slope of temperature (**a**), precipitation (**b**), and streamflow (**c**). Note: The single asterisks ("*"), two asterisks ("**"), and three asterisks ("***") represent statistical significance levels of $p < 0.1$, $p < 0.05$, and $p < 0.01$, respectively.

3.4. Hydrological Responses to Climate Change and LUCC

The SWAT model simulation results under the different scenarios show that the impacts of climate change and LUCC (S3) projected an increase in future streamflow for ZM River (Table 3b). Decreasing trends were noted for JT (Table 3a), HY (Table 3c), and GL Rivers (Table 3d). ZM River experienced an increase of 0.25 m^3/s, accounting for 3.85% of total streamflow, while JT, HY, and GL Rivers decreased by 0.29 m^3/s, 0.07 m^3/s, and 0.68 m^3/s, contributing 7.34%, 2.25%, and 31.05%, respectively.

Table 3. Annual streamflow change in JTR (**a**), ZMR (**b**), HYR (**c**) and GLR (**d**) Basins under basic scenario (S0), climate scenario (S1), LUCC scenario (S2), and comprehensive scenario (S3).

Scenario	Sig.	Climate	LUCC	*p* (mm)	Streamflow (m^3/s)	Sig.	Value	Proportion
(**a**) JT River streamflow change								
S0	$Q_{l_1}^{c_1}$	1985–2000	1990s	484.61	3.95			
S1	$Q_{l_1}^{c_2}$	2001–2016	1990s	492.72	3.64	Q_C	−0.35	118.97%
S2	$Q_{l_2}^{c_1}$	1985–2000	2010s	484.61	4.04	Q_l	0.06	−18.97%
S3	$Q_{l_2}^{c_2}$	2001–2016	2010s	492.72	3.66	ΔQ	−0.29	
(**b**) ZM River streamflow change								
S0	$Q_{l_1}^{c_1}$	1985–2000	1990s	523.24	6.49			
S1	$Q_{l_1}^{c_2}$	2001–2016	1990s	530.82	6.69	Q_C	0.21	84.00%
S2	$Q_{l_2}^{c_1}$	1985–2000	2010s	528.85	6.52	Q_l	0.04	16.00%
S3	$Q_{l_2}^{c_2}$	2001–2016	2010s	535.46	6.73	ΔQ	0.25	
(**c**) HY River streamflow change								
S0	$Q_{l_1}^{c_1}$	1985–2000	1990s	400.9	3.11			
S1	$Q_{l_1}^{c_2}$	2001–2016	1990s	402.46	3.07	Q_C	−0.05	71.43%
S2	$Q_{l_2}^{c_1}$	1985–2000	2010s	400.9	3.1	Q_l	−0.02	28.57%
S3	$Q_{l_2}^{c_2}$	2001–2016	2010s	402.46	3.04	ΔQ	−0.07	
(**d**) GL River streamflow change								
S0	$Q_{l_1}^{c_1}$	1989–2000	1990s	373.49	2.19			
S1	$Q_{l_1}^{c_2}$	2001–2006	1990s	378.61	2.18	Q_C	−0.15	21.32%
S2	$Q_{l_2}^{c_1}$	1989–2000	2010s	373.49	1.79	Q_l	−0.53	78.68%
S3	$Q_{l_2}^{c_2}$	2001–2006	2010s	378.61	1.51	ΔQ	−0.68	

In the climate change-only scenario (S1), ZM River streamflow was projected to rise by 0.21 m^3/s, contributing 84.00%. In contrast, JT, HY, and GL Rivers were expected to decline by 0.35 m^3/s, 0.05 m^3/s, and 0.15 m^3/s, with contributions of 118.9%, 71.43%, and 21.32%. Under the LUCC-only scenario (S2), ZM River streamflow increased by 0.04 m^3/s, contributing 16.00%, while JT, HY, and GL Rivers decreased by 0.06 m^3/s, 0.07 m^3/s, and 0.53 m^3/s, with contributions of −18.97%, 28.57%, and 78.68%. From the annual

streamflow perspective, the streamflow changes in JT River, ZM River, and HY River are primarily attributed to climate change, while the streamflow changes in GL River are mainly attributed to human activities.

Monthly analyses indicated (Figure 8) that LUCC had minimal impact on the monthly streamflow of JT, ZM, and HY Rivers, with fluctuations not exceeding 0.3 m^3/s. ZM River displayed stable monthly variations between -0.06 m^3/s and 0.04 m^3/s. Significant changes for JT River occurred from April to June, while HY River showed notable fluctuations in April and May. GL River's monthly change due to LUCC ranged from -0.69 m^3/s to -0.28 m^3/s, indicating a stronger impact compared to climate change. Overall, climate change primarily affects the monthly streamflow of JT, ZM, and HY Rivers during the summer and autumn seasons, while LUCC has a more significant impact on the monthly streamflow of GL River, particularly during the summer, autumn, and winter seasons.

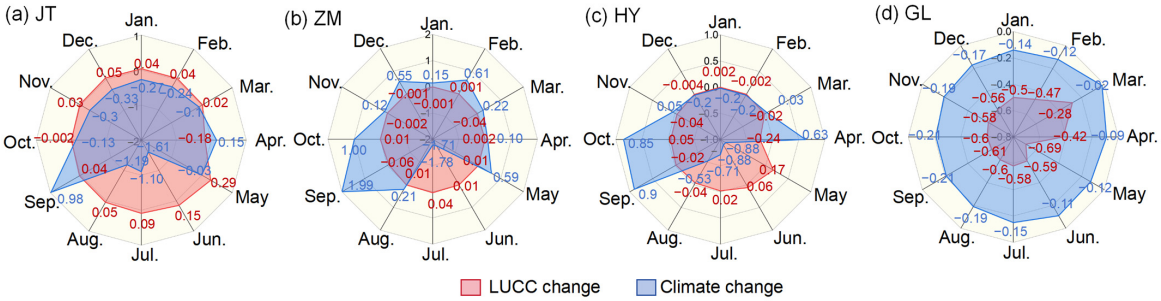

Figure 8. Changes in monthly streamflow impacted by climate change and LUCC in the JTR (**a**), ZMR (**b**), HYR (**c**), and GLR (**d**).

4. Discussion

4.1. Causes of Climate Change Impact on Streamflow

We proposed a research framework based on the SWAT model to quantify the impacts of climate change and human activities on streamflow, which helps to explain, to some extent, the driving mechanisms behind streamflow variation. Compared to studies that focus on a single variable [24,38–40], we considered both climate change and LUCC as the two primary hydrological drivers, enabling a more comprehensive attribution analysis of the complex, nonlinear streamflow variations. Our findings suggest that climate change accounts for approximately three-quarters of the streamflow variations in arid alpine regions, with temperature and precipitation serving as the primary climatic drivers. These factors contribute to shifts in streamflow distribution and an increase in hydrological variability [38,41]. Over the past 40 years, the annual average temperature and precipitation in the study area have increased to varying degrees, aligning with the climate change trends observed by Zeng et al. [39,42] in Northwest China at the end of the 20th century. This indicates an intensification of warming and wetting trends in the region. However, most river streamflow shows a declining trend, which corresponds to the findings of Zhao et al. and other scholars in arid plateau regions [33,38]. These phenomena may indicate a global climate shift towards arid conditions [43].

In arid alpine regions, changes in streamflow are predominantly linked to climate change. Yang et al. [31] found that climate change was responsible for more than 80% of the change in streamflow in the Heihe River, while Zeng et al. [44] identified climate change as the dominant factor affecting the Jialing River and Jinsha River. Similarly, our study also revealed that climate change contributes to more than 70% of the streamflow change in most rivers within the study area (e.g., JTR, ZMR, and HYR). Additionally, our results indicate that the contribution of climate change to streamflow change increases with elevation. This vertical zonation likely explains the differing impacts of climate change on streamflow, as its influence diminishes significantly in lower-altitude, flatter basins, a trend also observed in regions like the Himalayan Basin [45].

Precipitation shows a significant positive correlation with streamflow in these contexts (Table 4), indicating that in arid alpine regions, precipitation is the primary driver of change

in streamflow. However, the influence of temperature on streamflow is more complex. In the study area, streamflow mainly originates from precipitation and glacial melt [23]. Temperature affects streamflow through increased evaporation and changes in glacier melt dynamics [45]. Notably, as temperatures rise, streamflow tends to decrease after glacier melt peaks. This suggests that before peak melt, temperature and streamflow are positively correlated, but this relationship reverses afterward. This conclusion is supported by extensive data from the inland river in Northwest China [40,46]. Therefore, the significant increase in temperature and moderate rise in precipitation may lead to increased glacial melt in the ZM River, resulting in higher flow rates. Meanwhile, Li et al.'s study on the Yarlung Tsangpo River indicates that when rising temperatures cause evaporation to exceed the contributions from precipitation and glacial melt, streamflow will decrease [33]. Consequently, the reduction in streamflow observed in the JT, HY, and GL Rivers under climate change scenarios may be due to enhanced evaporation.

Table 4. Pearson correlations of precipitation and temperature with water flow in the JTR, ZMR, HYR, and GLR. Note: The single asterisk ("*") and two asterisks ("**"), represent statistical significance levels of $p < 0.1$and $p < 0.05$, respectively.

Basin		Pearson Correlation Coefficient	*p* Value	Sig.
JT River	Temperature	−0.32	0.08	
	Precipitation	0.62	<0.01	**
ZM River	Temperature	0.12	0.53	
	Precipitation	0.51	0.04	*
HY River	Temperature	−0.36	0.04	*
	Precipitation	0.81	<0.01	**
GL River	Temperature	−0.31	0.21	
	Precipitation	0.96	<0.01	**

4.2. Causes of LUCC Impact on Streamflow

The impact of human activities on streamflow is reflected through changes in LUCC closely associated with human activities, such as cultivated land and urban land [47,48]. Using the SWAT model, we translated the complex effects of human activities into more intuitive LUCC data for our analysis. The study emphasizes the significant role of LUCC in influencing streamflow variations in arid alpine regions. Substantial changes in surface properties, such as roughness and permeability, directly impacted hydrological processes like vegetation interception and soil water infiltration, thereby affecting streamflow dynamics [49,50]. Human activities and land management policies often initiated LUCC, making these alterations indirect results of human intervention [5]. Urbanization increased impervious surfaces, leading to enhanced streamflow, while reforestation and conversion of farmland to forest increased vegetation cover, which improved interception and evapotranspiration, consequently reducing streamflow [49].

LUCC as a key driver of streamflow change [47,48]. For example, Du et al. found that human activities are the main driving factor behind the reduction in streamflow of the Yongding River using the ABCD model [12], while Shi et al. quantified the impact of human activities on the streamflow of the Jialing River using the SWAT model, revealing that it exceeds 50% [13]. In our study area, the GL Basin exhibits the most significant LUCC, and these changes have the greatest contribution to streamflow dynamics. The LUCC driven by human activities in this region are primarily reflected in the areas of cultivated land and urban land. Therefore, our comparison of the GL River with three other rivers indicated that this conclusion is particularly relevant in areas with significant human disturbance. In arid alpine regions, areas with frequent human activity typically have gentle terrain and minimal climatic variation due to less pronounced vertical zonation. In these regions, streamflow generally decreased because of factors such as agricultural irrigation, domestic consumption, and industrial water use [51].

This combination of factors allowed human activities to exert a stronger influence on streamflow than climate change. In conclusion, while LUCC affects streamflow dynamics, its impact varies by region and is often exacerbated by human activities. This highlights the necessity for a nuanced understanding of these interactions in arid alpine environments.

4.3. Synergistic Effects of LUCC and Climate Change on Streamflow and Management Implications

This study demonstrated that the combined effects of LUCC and climate change resulted in more significant variations in streamflow for the HY, ZM, and GL River Basins than those observed under single-factor scenarios (S1 and S2). Notably, in the single climate change scenario (S1), the JT River Basin exhibited the most pronounced streamflow change. This finding underscores the complex interactions of multiple factors affecting the hydrological cycle, with differences largely attributed to the unique geographical characteristics of each basin [44].

For future water resource management, it is essential to acknowledge the sensitivity of high-altitude regions to climate change while fully considering the impact of human activities. This dual influence presents considerable challenges for the management of water resources. Additionally, accurately assessing streamflow in arid alpine regions is crucial, as it relates directly to maintaining ecological base flows and ensuring the health and stability of the water cycle [52–54].

Therefore, we recommend establishing effective early-warning systems for climate and hydrological monitoring in arid alpine regions, along with maintaining long-term streamflow records. These measures are key to achieving effective water resource management [55]. Land monitoring and the development of sustainable land policies are crucial [56]. Most of the study area is located within the Qilian Mountain National Park. Effectively coordinating vegetation restoration with human activities will bring significant benefits in alleviating water resource shortages in the watershed. Furthermore, to enhance research on water resource management in these regions, future efforts should integrate ecological and hydrological engineering factors for a more comprehensive understanding of hydrological changes. It is also vital to refine existing models by incorporating modules for snowmelt and permafrost simulation and utilizing higher-resolution remote sensing imagery to improve model applicability [57]. Future streamflow management policies will emphasize the coordinated development of climate change and LUCC [58]. There exists an interactive relationship between climate and land. By enhancing vegetation restoration within the watershed, increasing surface retention, controlling emissions, and mitigating the trend of rising temperatures, we can effectively alleviate the water resource conflicts in arid mountainous regions (Figure 9).

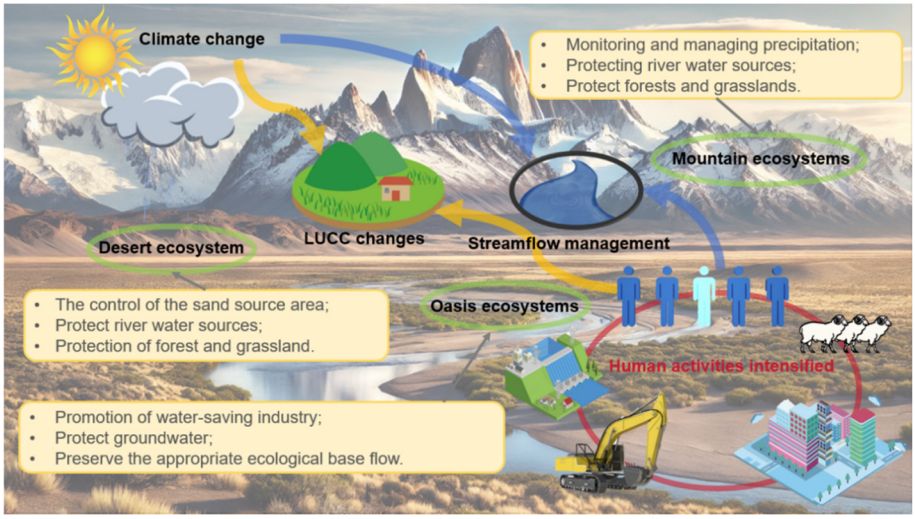

Figure 9. Streamflow suitability management in arid alpine regions.

4.4. Limitations

This study established a quantitative analytical framework to assess the impacts of climate change and human activities on streamflow in arid alpine regions. However, because of the limited number of observation stations in these areas., it was challenging to obtain additional critical hydrometeorological data (e.g., dew point and solar radiation) needed to drive the model. Furthermore, the absence of relevant data from upstream hydropower stations led to the exclusion of the effects of hydraulic structures on streamflow, thereby limiting the model's simulation performance [31].

The ecological fragility and complex terrain of arid alpine basins mean that streamflow is closely related to topography, vegetation cover, soil conditions, climate change, and human activities. In our analysis, we primarily focused on climate and LUCC as the two most significant factors. However, this focus was insufficient to fully reveal the physical mechanisms governing the hydrological cycle in arid alpine regions [55,57]. Additionally, our research framework is also applicable to studies related to the water cycle, such as evapotranspiration and soil water [31]. However, the research framework for the hydrological cycle in arid alpine regions still has room for further improvement. In summary, while the framework provided valuable insights, the limitations imposed by data availability and the complexity of environmental interactions highlight the need for more comprehensive research. Future studies should aim to incorporate additional hydrometeorological variables and consider the influences of hydraulic infrastructure more thoroughly. A broader perspective that encompasses other environmental factors is essential for a complete understanding of the hydrological dynamics in these sensitive regions.

5. Conclusions

This study developed a research framework based on the SWAT model (Figure 2) to attribute change in streamflow to climate change and human interventions while quantifying their contributions. By addressing four critical questions, it provided important insights for both academia and policymakers:

(1) Over the past 40 years, temperature and precipitation in arid alpine regions have consistently increased. Although the warming trend has been significant, it has slowed in recent years. However, the streamflow of three out of four rivers has shown a declining trend (i.e., JTR, HYR, and GLR).
(2) The land types within the watershed were relatively stable, with LUCC mainly occurring in the GLR watershed. This was primarily characterized by a reduction in grassland and an increase in cultivated land, while the comprehensive land use dynamic degrees in the remaining sub-watersheds were all less than 0.05%.
(3) Climate change has led to alterations in streamflow across most areas of arid mountainous regions, particularly in high and rugged terrains (i.e., JTR, ZMR, and HYR). In these areas, the impact of climate change on streamflow change exceeds 70%. Specifically, the impact of climate change on streamflow in JTR, ZMR, and HYR is 118.97%, 84.00%, and 71.43%, respectively.
(4) LUCC associated with human activities have led to increased water consumption, resulting in reduced streamflow, particularly in low-lying and gently undulating areas (i.e., GLR). In GLR, changes in streamflow due to LUCC account for 78.68%.

The findings indicate that as human activities have intensified and temperatures have continued to rise, streamflow is projected to decline further. This situation necessitates urgent and effective water resource management measures to alleviate water scarcity. Additionally, the research highlights the complex interactions among multiple factors influencing the hydrological cycle in arid regions. It underscores the urgent need to enhance the monitoring of meteorological and hydrological changes to address the challenges posed by climate change in these areas.

Supplementary Materials: The following supporting information can be downloaded at https://www.mdpi.com/article/10.3390/land13111961/s1, Table S1: Abbreviation Decoding of Nouns; Table S2: Value of SWAT model parameters; Table S3: Data Sources and Description. References [59,60] are cited in the supplementary materials.

Author Contributions: Conceptualization, H.X., L.Y. and Q.F., methodology, H.X. and Y.S., software, H.X., validation, L.Y., Y.S. and Q.F., formal analysis, H.X., L.Y. and Y.S., investigation, W.L. and Q.F., resources, H.X., L.Y. and Q.F., data curation, H.X. and Y.S., writing—original draft preparation, H.X., Q.F. and Y.S., writing—review and editing, H.X., Q.F. and L.Y., visualization, H.X., L.Y. and W.L., supervision, L.Y., Q.F. and J.M. All authors have read and agreed to the published version of the manuscript.

Funding: This research has been funded by the Strategic Priority Research Program of CAS (Grant No. XDB0720202), the National Natural Science Fund of China (Grant No. 52379030 and 52179026), the National Key R&D Program of China (Grant No. 2022YFF1303301 and 2022YFF1302603), the Gansu Provincial Science and Technology Planning Project (Grant No. 24JRRA079), the Youth Innovation Promotion Association of CAS (Grant No. 2022435), the Young Elite Scientist Sponsorship Program of CAST (Grant No. YESS20200089), and the Natural Science Foundation of Gansu Province (Grant No. 22JR5RA072).

Data Availability Statement: The original contributions presented in this study are included in the Supplementary Material. Further inquiries can be directed to the corresponding author.

Conflicts of Interest: The authors declare that they have no known competing financial interests or personal relationships that could have appeared to influence the work reported in this paper.

References

1. Li, C.; Fu, B.; Wang, S.; Stringer, L.C.; Wang, Y.; Li, Z.; Liu, Y.; Zhou, W. Drivers and impacts of changes in China's drylands. *Nat. Rev. Earth Environ.* **2021**, *2*, 858–873. [CrossRef]
2. Lian, X.; Piao, S.; Chen, A.; Huntingford, C.; Fu, B.; Li, L.; Huang, J.; Sheffield, J.; Berg, A.M.; Keenan, T.F.; et al. Multifaceted characteristics of dryland aridity changes in a warming world. *Nat. Rev. Earth Environ.* **2021**, *2*, 232–250. [CrossRef]
3. Liu, L.; Gou, X.; Wang, X.; Yang, M.; Qie, L.; Pang, G.; Wei, S.; Zhang, F.; Li, Y.; Wang, Q.; et al. Relationship between extreme climate and vegetation in arid and semi-arid mountains in China: A case study of the Qilian Mountains. *Agric. For. Meteorol.* **2024**, *348*, 109938. [CrossRef]
4. Zhang, P.; Cai, Y.; He, Y.; Xie, Y.; Zhang, X.; Li, Z. Changes of vegetational cover and the induced impacts on hydrological processes under climate change for a high-diversity watershed of south China. *J. Environ. Manag.* **2022**, *322*, 115963. [CrossRef]
5. Tan, X.; Gan, T. Contribution of human and climate change impacts to changes in streamflow of Canada. *Sci. Rep.* **2015**, *5*, 17767. [CrossRef]
6. Sha, Z.; Bofu, Y.; Lintner Benjamin, R.; Kirsten, L.; Zhang, Y. Projected increase in global runoff dominated by land surface changes. *Nat. Clim. Chang.* **2023**, *13*, 442–449.
7. Sadra, N.; Nikoo, M.R.; Talebbeydokhti, N. Non-stationary evaluation of runoff peaks in response to climate variability and land use change in Ferson Creek, Illinois, USA. *Environ. Monit. Assess.* **2023**, *195*, 661. [CrossRef]
8. Kuang, W.; Liu, J.; Dong, J.; Chi, W.; Zhang, C. The rapid and massive urban and industrial land expansions in China between 1990 and 2010: A cloud-based analysis of their trajectories, patterns, and drivers. *Landsc. Urban Plan.* **2016**, *145*, 21–33. [CrossRef]
9. Hu, Y.; Duan, W.; Chen, Y.; Zou, S.; Kayumba, P.M.; Sahu, N. An integrated assessment of runoff dynamics in the Amu Darya River Basin: Confronting climate change and multiple human activities, 1960–2017. *J. Hydrol.* **2021**, *603*, 126905. [CrossRef]
10. World Meteorological Organization 2023. State of Global Water Resources 2023. United Nations World Water Development Report. Retrieved October 2023. Available online: https://www.unwater.org/news/wmo-state-global-water-resources-2023 (accessed on 1 October 2024).
11. Wang, R.; Xiong, L.; Xu, X.; Liu, S.; Feng, Z.; Wang, S.; Huang, Q.; Huang, G. Long-term responses of the water cycle to climate variability and human activities in a large arid irrigation district with shallow groundwater: Insights from agro-hydrological modeling. *J. Hydrol.* **2023**, *626*, 130264. [CrossRef]
12. Wang, A.; Miao, Y.; Kong, X.; Wu, H. Future changes in global runoff and runoff coefficient from CMIP6 multi-model simulation under SSP1-2.6 and SSP5-8.5 scenarios. *Earth's Future* **2022**, *10*, e2022EF002910. [CrossRef]
13. Ansarifard, S.; Ghorbanifard, M.; Boustani, F.; Abdolazimi, H. Hydrological simulation and evaluation of drought conditions in the ungauged watershed of Parishan Lake, Iran, using the SWAT model. *J. Water Clim. Chang.* **2024**, *15*, 4666–4698. [CrossRef]
14. Du, Y.; Bao, A.; Zhang, T.; Ding, W. Quantifying the impacts of climate change and human activities on runoff variation: Case study of the upstream of Minjiang River, China. *Ecol. Indic.* **2023**, *154*, 110839. [CrossRef]
15. Shi, W.; He, Y.; Shao, Y. Effects of climate change and human activities on runoff in the upper reach of Jialing River, China. *Remote Sens.* **2024**, *16*, 2481. [CrossRef]

16. Miao, C.; Wu, Y.; Fan, X.; Su, J. Projections of global land runoff changes and their uncertainty characteristics during the 21st century. *Earth's Future* **2023**, *1*, e2022EF003286. [CrossRef]
17. Zhou, S.; Yu, B.; Zhang, L.; Huang, Y.; Pan, M.; Wang, G. A new method to partition climate and catchment effect on the mean annual runoff based on the Budyko complementary relationship. *Water Resour. Res.* **2016**, *52*, 7163–7177. [CrossRef]
18. Yang, L.; Zhao, G.; Tian, P.; Mu, X.; Tian, X.; Feng, J.; Bai, Y. Runoff changes in the major river basins of China and their responses to potential driving forces. *J. Hydrol.* **2022**, *607*, 127536. [CrossRef]
19. Zuo, G.; Luo, J.; Wang, N.; Lian, Y.; He, X. Decomposition ensemble model based on variational mode decomposition and long short-term memory for streamflow forecasting. *J. Hydrol.* **2020**, *585*, 124776. [CrossRef]
20. Kåresdotter, E.; Destouni, G.; Ghajarnia, N.; Lammers, R.B.; Kalantari, Z. Distinguishing direct human-driven effects on the global terrestrial water cycle. *Earth's Future* **2022**, *10*, e2022EF002848. [CrossRef]
21. Ellis, C.R.; Pomeroy, J.W.; Brown, T.; MacDonald, J. Simulation of snow accumulation and melt in needleleaf forest environments. *Hydrol. Earth Syst. Sci.* **2010**, *14*, 925–940. [CrossRef]
22. Leng, G.; Tang, Q.; Rayburg, S. Climate change impacts on meteorological, agricultural and hydrological droughts in China. *Glob. Planet. Chang.* **2015**, *126*, 23–34. [CrossRef]
23. Liu, Y.; Liu, F.; Chen, C.; Chen, Q.; Zhang, J.; Mo, K.; Jiang, Q.; Yao, S. A holistic approach to projecting streamflow and analyzing changes in ecologically relevant hydrological indicators under climate and land use/cover change. *J. Hydrol.* **2024**, *632*, 130863. [CrossRef]
24. Tan, M.; Gassman, P.; Yang, X.; Haywood, J. A review of SWAT applications, performance and future needs for simulation of hydro-climatic extremes. *Adv. Water Resour.* **2020**, *143*, 103662. [CrossRef]
25. He, Z.; Pomeroy, J.W.; Fang, X.; Peterson, A. Sensitivity analysis of hydrological processes to perturbed climate in a southern boreal forest basin. *J. Hydrol.* **2021**, *601*, 126706. [CrossRef]
26. Huang, C.; Zhang, Y.; Hou, J. Soil and Water Assessment Tool (SWAT)-informed deep learning for streamflow forecasting with remote sensing and in situ precipitation and discharge observations. *Remote Sens.* **2024**, *16*, 3999. [CrossRef]
27. Huss, M.; Hock, R. Global-scale hydrological response to future glacier mass loss. *Nat. Clim. Chang.* **2018**, *8*, 135–140. [CrossRef]
28. Mohammadzadeh, H.; Sori, R.; Heydarizad, M. The contribution of moisture sources of precipitation to water resources recharge in semi-arid regions. *Atmosphere* **2024**, *15*, 1274. [CrossRef]
29. Zafar, U.; Anjum, M.N.; Hussain, S.; Sultan, M.; Rasool, G.; Bin Riaz, M.Z.; Shoaib, M.; Asif, M. Analyzing the spatiotemporal changes in climatic extremes in cold and mountainous environments: Insights from the Himalayan Mountains of Pakistan. *Atmosphere* **2024**, *15*, 1221. [CrossRef]
30. Li, X.; Wang, Y.; Zhao, Y.; Zhai, J.; Liu, Y.; Liul, K. Research on the impact of climate change and human activities on the NDVI of arid areas—A case study of the Shiyang River Basin. *Land* **2024**, *13*, 533. [CrossRef]
31. Yang, L.; Feng, Q.; Yin, Z.; Wen, X.; Si, J.; Li, C.; Deo, R.C. Identifying separate impacts of climate and land use/cover change on hydrological processes in upper stream of Heihe River, Northwest China. *Hydrol. Process.* **2017**, *31*, 1100–1112. [CrossRef]
32. Hamed, K.H. Trend detection in hydrologic data: The Mann-Kendall trend test under the scaling hypothesis. *J. Hydrol.* **2008**, *349*, 350–363. [CrossRef]
33. Li, C.; Hao, J.; Zhang, G.; Fang, H.; Wang, Y.; Lu, H. Runoff variations affected by climate change and human activities in Yarlung Zangbo River, southeastern Tibetan Plateau. *Catena* **2023**, *230*, 107184. [CrossRef]
34. Williams, S. Pearson's correlation coefficient. *N. Z. Med. J.* **1996**, *109*, 38. [PubMed]
35. Ayenew, D.A.; Paul, D.W.; Dejene, S.; Nicola, F. Land use change and climate dynamics in the Rift Valley Lake Basin, Ethiopia. *Environ. Monit. Assess.* **2022**, *194*, 791.
36. Liu, J.; Kuang, W.; Zhang, Z.; Xu, X.; Qin, Y.; Ning, J.; Zhou, W.; Zhang, S.; Li, R.; Yan, C.; et al. Spatiotemporal characteristics, patterns, and causes of land use changes in China since the late 1980s. *Acta Geogr. Sin.* **2014**, *24*, 195–210. [CrossRef]
37. Yuan, Y.; Koropeckyj-Cox, L. SWAT model application for evaluating agricultural conservation practice effectiveness in reducing phosphorous loss from the Western Lake Erie Basin. *J. Environ. Manag.* **2022**, *302*, 114000. [CrossRef]
38. Zhao, J.; Huang, Q.; Chang, J.; Liu, D.; Huang, S.; Shi, X. Analysis of temporal and spatial trends of hydro-climatic variables in the Wei River Basin. *Environ. Res.* **2015**, *139*, 55–64. [CrossRef]
39. Zeng, P.; Sun, F.; Liu, Y.; Feng, H.; Zhang, R.; Che, Y. Response of potential evapotranspiration to warming and wetting in Northwest China. *Atmosphere* **2022**, *13*, 353. [CrossRef]
40. Wang, T.; Yang, D.; Yang, Y.; Zheng, G.; Jin, H.; Li, X.; Yao, T.; Cheng, G. Unsustainable water supply from thawing permafrost on the Tibetan Plateau in a changing climate. *Sci. Bull.* **2023**, *68*, 1105–1108. [CrossRef]
41. Peng, Y.; He, G.; Wang, G.; Cao, H. Surface water changes in Dongting Lake from 1975 to 2019 based on multisource remote-sensing images. *Remote Sens.* **2021**, *13*, 1827. [CrossRef]
42. Yang, J.; Zhang, Q.; Lu, G.; Liu, X.; Zhu, B. Climate transition from warm-dry to warm-wet in eastern Northwest China. *Atmosphere* **2021**, *12*, 548. [CrossRef]
43. Yuan, X.; Wang, Y.; Ji, P.; Wu, P.; Sheffield, J.; Otkin, J.A. A global transition to flash droughts under climate change. *Science* **2023**, *380*, 187–191. [CrossRef] [PubMed]
44. Zeng, F.; He, Q.; Li, Y.; Shi, W.; Yang, R.; Ma, M.; Huang, G.; Xiao, J.; Yang, X.; Di, D. Reduced runoff in the upper Yangtze River due to comparable contributions of anthropogenic and climate changes. *Earth's Future* **2024**, *12*, 7. [CrossRef]

45. Xiang, Y.; Zeng, C.; Zhang, F.; Wang, L. Effects of climate change on runoff in a representative Himalayan basin assessed through optimal integration of multi-source precipitation data. *J. Hydrol. Reg. Stud.* **2024**, *53*, 101828. [CrossRef]
46. Jia, Y.; Li, Z.; Gao, H.; Wang, S.; Sun, M.; Wang, P. Hydrological response to climate change in a glacierized catchment in eastern Tien Shan, Central Asia. *J. Hydrol. Reg. Stud.* **2024**, *51*, 101669. [CrossRef]
47. Li, J.; Chen, Y.; Gu, Y.; Wang, M.; Zhao, Y. Remote sensing mapping and analysis of spatiotemporal patterns of land use and cover change in the Helong region of the Loess Plateau (1986–2020). *Remote Sens.* **2024**, *16*, 3738. [CrossRef]
48. Yang, X.; Gu, X.; Zhang, P.; Liu, J.; Zhang, W.; Long, A. Assessment of the impacts of climate and land use changes on water yield in the Ebinur Lake Basin. *Land* **2024**, *13*, 1324. [CrossRef]
49. Cheng, Y.; Chen, Y. Spatial and Temporal Characteristics of Land Use Changes in the Yellow River Basin from 1990 to 2021 and Future Predictions. *Land* **2024**, *13*, 1510. [CrossRef]
50. Sajikumar, N.; Remya, R.S. Impact of land cover and land use change on runoff characteristics. *J. Environ. Manag.* **2015**, *161*, 460–468. [CrossRef]
51. Liu, H.; Chen, Y.; Du, P.; Wang, Y.; Zhao, Y.; Qu, L. Analysis of the changes and causes of runoff and sediment load in the middle reaches of the Yellow River from 1950 to 2022. *Land* **2024**, *13*, 1482. [CrossRef]
52. Chi, H.; Wu, Y.; Zheng, H.; Zhang, B.; Sun, Z.; Yan, J.; Ren, Y.; Guo, L. Spatial patterns of climate change and associated climate hazards in Northwest China. *Sci. Rep.* **2023**, *13*, 10418. [CrossRef] [PubMed]
53. Cui, B.; Gui, D.; Liu, Q.; Abd-Elmabod, S.K.; Liu, Y.; Lu, B. Distribution and growth drivers of oases at a global scale. *Earth's Future* **2024**, *12*, e2023EF004086. [CrossRef]
54. Feng, Q.; Yang, L.; Deo, R.C.; Aghakouchak, A.; Adamowski, J.F.; Stone, R.; Yin, Z.; Liu, W.; Si, J.; Wen, X.; et al. Domino effect of climate change over two millennia in ancient China's Hexi Corridor. *Nat. Sustain.* **2019**, *2*, 957–961. [CrossRef]
55. Dogan, F.; Karpuzcu, M.; Dogan, F.; Karpuzcu, M. Modeling fate and transport of pesticides from dryland agriculture using SWAT model. *J. Environ. Manag.* **2023**, *334*, 117457. [CrossRef]
56. Yang, L.; Feng, Q.; Ning, T.; Lu, T.; Zhu, M.; Yin, X.; Wang, J. Attributing streamflow variation by incorporating glacier mass balance and frozen ground into the Budyko framework in alpine rivers. *J. Hydrol.* **2024**, *628*, 130438. [CrossRef]
57. Fang, J.; Yang, L.; Wen, X.; Yu, H.; Li, W.; Adamowski, J.F.; Barzegar, R. Ensemble learning using multivariate variational mode decomposition based on the transformer for multistep-ahead streamflow forecasting. *J. Hydrol.* **2024**, *636*, 131275. [CrossRef]
58. Landry, J.-S.; Ramankutty, N. Carbon cycling, climate regulation, and disturbances in Canadian Forests: Scientific principles for management. *Land* **2015**, *4*, 83–118. [CrossRef]
59. Janjić, J.; Tadić, L. Fields of application of SWAT hydrological model—A review. *Earth* **2023**, *4*, 331–344. [CrossRef]
60. Zhang, Z.; Wang, Q.; Guan, Q.; Xiao, X.; Mi, J.; Lv, S. Research on the optimal allocation of agricultural water and soil resources in the Heihe River Basin based on SWAT and intelligent optimization. *Agric. Water Manag.* **2023**, *279*, 108177. [CrossRef]